Journal of Power Sources 241 (2013) 373–378

Contents lists available at SciVerse ScienceDirect

Journal of Power Sources

journal homepage: www.elsevier.com/locate/jpowsour

A dual function of high performance counter-electrode for stable quasi-solid-state dye-sensitized solar cells

Yaoming Xiao [a], Jihuai Wu [a,*], Jeng-Yu Lin [b], Gentian Yue [a], Jianming Lin [a], Miaoliang Huang [a], Zhang Lan [a], Leqing Fan [a]

[a] Institute of Materials Physical Chemistry, Huaqiao University, Quanzhou 362021, PR China
[b] Department of Chemical Engineering, Tatung University, Taipei 104, Taiwan

HIGHLIGHTS

- PEDOT–PAA–PSS is prepared and used as counter electrode in dye-sensitized solar cell.
- The hybrid can store liquid electrolyte and has good electrocatalytic activity.
- The efficiency of the solar cell using the dual function electrode reaches 6.35%.

ARTICLE INFO

Article history:
Received 3 December 2012
Received in revised form
26 March 2013
Accepted 20 April 2013
Available online 9 May 2013

Keywords:
Poly(3,4-ethylenedioxythiophene)
Poly(acrylic acid)
Counter electrode
Quasi-solid-state electrolyte
Dye-sensitized solar cell

ABSTRACT

A dual function polymer hybrid material poly(3,4-ethylenedioxythiophene) (PEDOT)–poly(acrylic acid) (PAA)–poly(styrenesulfonate) (PSS) was fabricated both as a counter electrode (CE) for I_3^- reduction and for storage of the liquid electrolyte in quasi-solid-state dye-sensitized solar cells (QS-DSSCs). To enhance the electrocatalytic activity of the nano-PEDOT CE and to improve the ionic conductivity of the three-dimensional (3D) PAA–PSS network, the columnar PEDOT was electropolymerized through the 3D PAA–PSS network. The QS-DSSC showed a high photovoltaic conversion efficiency of 6.35% under full sunlight illumination (100 mW cm^{-2}, AM1.5 G), which reduced to 6.03% after 100 days, indicating this QS-DSSC had a relatively good long-term stability.

1. Introduction

Since the first publication on dye-sensitized solar cells (DSSCs) by O' Regan and Grätzel in 1991 [1], the cells have attracted a great deal attention due to their low cost, simple preparation procedures, and relatively high energy conversion efficiency [2–4]. A typical DSSC consists of a dye-sensitized TiO_2 photoanode, a redox electrolyte, and a platinized counter electrode (CE). The CE should catalyze the reduction of I_3^- to I^-. To date, poly(3,4-ethylenedioxythiophene) (PEDOT) [5–8] has been investigated as a stable, highly conductive and more cost-effective CE replacing platinum [9] since Yohannes and Inganäs [10] reported that doped PEDOT can catalyze the I_3^-/I^- redox couple.

The DSSC electrolyte provides internal ionic conductivity within the porous nanocrystalline TiO_2 film [11] and is an important factor in determining the cell performance. Despite the high conversion efficiencies achieved for the DSSCs with liquid electrolytes, potential problems such as the leakage and volatilization of organic solvents in liquid electrolytes, are considered as some of the critical factors limiting the long-term performance and practical use of DSSCs [12–14]. Thus, all-solid-state electrolytes [15–18], ionic liquid electrolytes [19,20], and quasi-solid-state electrolytes [12,13,21–24] have been proposed as alternatives to liquid electrolytes. Among them, polymer gel electrolytes are considered as a substitute for liquid electrolytes, due to their high ionic conductivity, good interfacial filling properties, and relatively high long-term stability [25]. Cells using these electrolytes may be termed quasi-solid-state dye-sensitized solar cells (QS-DSSCs). Recently, polymer gel electrolytes based on a super-absorbent polymer poly(acrylic acid) (PAA) have been reported [13]. In it, either the carboxyl groups are modified or amphiphilic groups (e.g.,

* Corresponding author. Tel.: +86 595 22693899; fax: +86 595 22692229.
E-mail address: jhwu@hqu.edu.cn (J. Wu).

0378-7753/$ – see front matter © 2013 Elsevier B.V. All rights reserved.
http://dx.doi.org/10.1016/j.jpowsour.2013.04.091

polyethylene glycol [12,13], glycerin [26], *g*-cetyltrimethyl ammonium bromide [27], or gelatin [28]) are introduced to improve organic solvent absorbency. Introduction of conducting polymers (e.g., polypyrrole [22] or polyaniline [24]) enhances electron conductivity in the polymer hybrid. Such polymer hybrids showed excellent stability and liquid electrolyte absorbent ability, and were used to form high performance, stable QS-DSSCs.

In this paper, we report a novel dual function organic polymer hybrid material PEDOT–PAA–poly(styrenesulfonate) (PSS) prepared using pulse potentiostatic electropolymerization of high-uniformity nano-PEDOT film on a fluorinated tin oxide (FTO) substrate. It was then subjected to sequential chemical redox polymerization of a microporous PAA–PSS thin film, which was used as the CE for I_3^- reduction and for storage for the liquid electrolyte in the QS-DSSC. The latter achieved the relatively high energy conversion efficiency of 6.35%, which fell to 6.03% after 100 days, showing that this QS-DSSC had a relatively good long-term stability.

2. Experimental

2.1. Fabrication of CEs

Pulse potentiostatic electropolymerization [7,8] of PEDOT onto cleaned FTO glass substrates (13 Ω $\square^{-1}$, NSG) were carried out using a Zahner electrochemical workstation (Germany) from a simple three compartment deposition bath containing 2.0 mM 3,4-ethylenedioxythiophene monomer (99% EDOT, ARCOS), 10 mM poly(styrenesulfonate) (PSS), and 10 mM lithium perchlorate ($LiClO_4$) in aqueous solution (called here EDOT aqueous solution) at ambient atmosphere. Preparative parameters for PEDOT CEs were selected as 1.2 V imposed pulse potential, 0.2 V pulse-reversal potential, 1 s pulse period, 0.5 s pulse-reversal period, and total 500 s duration time. Cleaned FTO glass substrates and a Pt wire were used as working electrodes and as the counter electrode, respectively, with a saturated silver/silver chloride (Ag/AgCl) reference electrode. The PEDOT CEs thus obtained were rinsed in distilled water and dried under a cool air flow.

The oligo–PAA–PSS hybrid was prepared by the following processes. First, 10 ml acrylic acid monomer, 3.0 g PSS, with 0.01 g *N*,*N*′-methylenebisacrylamide as cross-linker agent were dissolved in 12 ml deionized water with stirring. Second, 0.1 g ammonium persulfate used as a redox initiator for the PAA polymerization reaction was added drop-wise into the above mixture at 4 °C under vigorous stirring to form homogeneous oligo–PAA–PSS hybrid polymer.

The product was coated onto the PEDOT CEs to form PEDOT–PAA–PSS (further abbreviated as P-0) CEs by the doctor blade technique. Polymerization was allowed to take place at 80 °C for 30 min under nitrogen atmosphere. The resultant was washed at room temperature in excess deionized water to remove impurities, and vacuum-dried at 80 °C for 2 h. P-0 CEs were immersed in the above EDOT aqueous solution for 6 h. Electropolymerization of PEDOT onto the P-0 CE was then carried out using the method described for FTO over periods of 500, 1000, and 1500 s. The P-0, P-500, P-1000, and P-1500 CEs obtained were rinsed in deionized water to remove any impurities and freeze-dried (FD-1A-50, China).

2.2. Characterization

The surface features of samples were observed using scanning electron microscopes (SEM, JSM-7600F and S-3500N). Fourier transform infrared spectra (FTIR) of samples were recorded on a Nicolet Impact 410 FTIR spectrophotometer (UK) with KBr cut-off. Cyclic voltammogram (CV) for the I^-/I_3^- system used an electrolyte consisting of 50 mM LiI, 10 mM I_2, and 500 mM $LiClO_4$ dissolved in a 2:8 by volume mixture of *N*-methyl-2-pyrrolidone (NMP, ARCOS) and 3-methoxypropionitrile (3-MPN, ARCOS). Results were obtained in the potential range −0.4 V to 0.4 V at a scan rate of 10 mV s^{-1} using a computer-controlled potentiostat (PGSTAT320N, Autolab). A three-electrode electrochemical cell was used, containing the CEs obtained as working electrodes, a Pt-foil counter electrode, and a Pt wire reference electrode. The symmetrical dummy cells (shown in Fig. 1a–c) were used for the electrochemical impedance spectroscopy (EIS) and Tafel polarization measurements. The EIS measurements were conducted by using the Zahner electrochemical workstation. The impedance studies were carried out simulating open-circuit conditions in the dark under ambient atmosphere, and the impedance data covered a frequency range of 10^{-1}–10^6 Hz with zero bias potential, and at 10 mV signal amplitude. The resulting impedance spectra were analyzed by means of Z-view software. Tafel polarization curves were measured using an electrochemical workstation system (CHI660D, China) at a scan rate of 10 mV s^{-1}.

The redox electrolyte used for EIS, Tafel polarization, and photovoltaic conversion measurements consisted of 1 M 1,3-dimethylimidazolium iodide (Merck), 0.5 M 4-tert-butyl-pyridine (Aldrich), 0.15 M iodine (J.T. Baker), and 0.1 M guanidine thiocyanate (Aldrich) in a 2:8 NMP and 3-NMP mixture. The CV, EIS, Tafel polarization, and photovoltaic conversion measurements were obtained after the samples were immersed in the corresponding test solution for 24 h to absorb electrolytes adequately.

2.3. Measurement

The absorbency (g g^{-1}) of each sample was measured according to the equation below [29]:

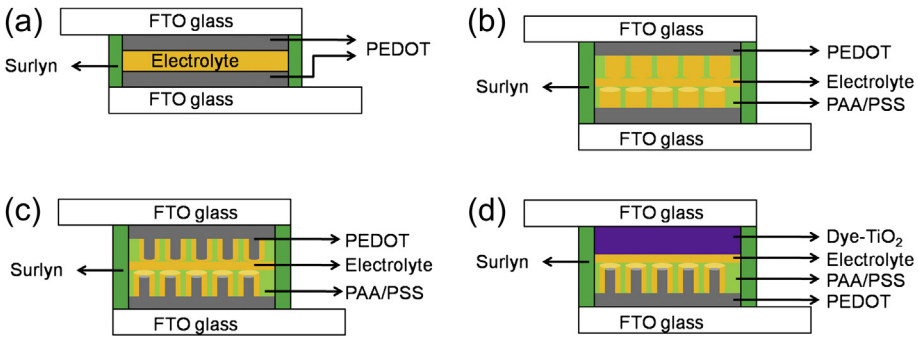

Fig. 1. Symmetric dummy cells (a, b, and c) used for EIS and Tafel polarization measurements, schematic diagram of the QS-DSSC (d).

$$\text{Absorbency} = (W_2 - W_1)/W_1 \quad (1)$$

where W_1 is the mass of dried sample (g), W_2 is the mass of the sample swollen with electrolyte (g). The ionic conductivity of the quasi-solid-state electrolyte was measured by using a digitized conductivity meter (DDSJ-308A, China). The instrument was calibrated with 0.01 M KCl aqueous solution prior to experiments [13].

2.4. Photoelectrochemical testing

TiO_2 colloid and TiO_2 photoanode were prepared as reported previously [12,13,30]. The latter was sensitized by immersing it into a 0.3 mM ethanolic solution of N719 dye ([cis-di(thiocyanato)-*N*,*N*′-bis(2,2′-bipyridyl-4-carboxylic acid-4-tetrabutylammonium carboxylate) ruthenium (II)]; Everlight Chemical Industry Co.) for 4 h, followed by air drying. After dye adsorption, TiO_2 photoanode was assembled with a CE (shown in Fig. 1d) in a 30 μm spacer made by a thermobonding surlyn film (Dupont). Then the liquid electrolyte was injected into the cell. The photocurrent density–voltage characteristic was made using a computer-controlled Keithley 2400 source meter under illumination by a solar simulator (Yamashita Denso YSS-150A). The incident light intensity and the active cell area were 100 mW cm^{-2} (AM1.5) and 0.28 cm^2, respectively.

3. Results and discussion

3.1. Morphology and compositions

Fig. 2a-1 and a-2 demonstrate a high-uniformity nano-PEDOT CE prepared by using the pulse potentiostatic method. For the P-0 CE (Fig. 2b), it can be found that three-dimensional (3D) PAA–PSS network was fabricated onto the nano-PEDOT CE. To enhance the electrocatalytic activity of the PEDOT CEs for I_3^- reduction and to improve the ionic conductivity of the 3D PAA–PSS network, electropolymerization of columnar PEDOT was carried out onto the nano-PEDOT thin film and passed through the 3D PAA–PSS network. The columnar PEDOT continuously grew with increasing the duration time of PEDOT electropolymerization. After 1000 s duration time, the 3D PAA–PSS network was properly filled up with the columnar PEDOT (Fig. 2d). However, Fig. 2e illustrates the columnar PEDOT became oversize after 1500 s duration time, which would obviously reduce the inner space for absorbing the liquid electrolyte. Thus the best duration time was set as 1000 s.

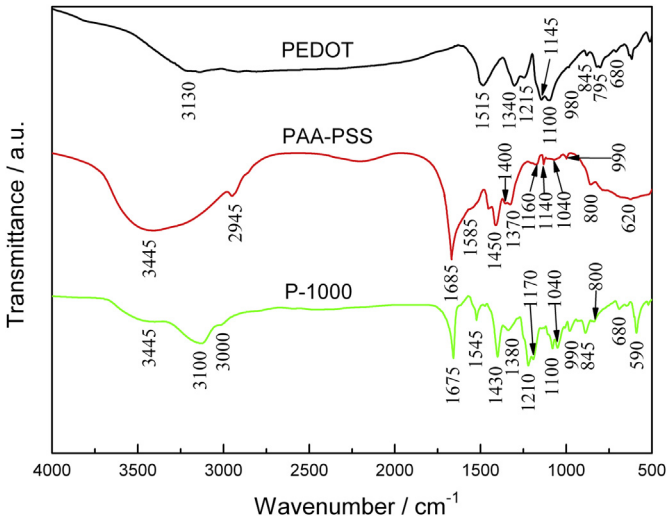

Fig. 3. FTIR spectra of the PEDOT, PAA–PSS, and P-1000, respectively.

Fig. 3 shows the FTIR spectra of the PEDOT, PAA–PSS, and P-1000, respectively. As shown in the PEDOT curve, the vibrations at 1340 and 1515 cm^{-1} can be attributed to the C–C and C=C stretching of the quinoidal structure of the thiophene ring [31]. The vibrations at 1215, 1145 and 1100 cm^{-1} possibility originate from to the C–O–C bond stretching in the ethylene dioxy group [32]. The C–S bond stretching in the thiophene ring is also seen at 980, 845, and 680 cm^{-1} [33]. For the PAA–PSS curve, a middle strong and broad absorption band at 3445 cm^{-1} arises from the O–H stretching mode in PAA polymer. The absorption peak at 2945 cm^{-1} responses for the $-CH_3$, and the band centers at 1450, 1400, 800, and 620 cm^{-1} arise from the $-CH_2-$ wagging vibration, $-CH_3$ scissoring vibrations, C–H out-of-plane bending vibration, and C–

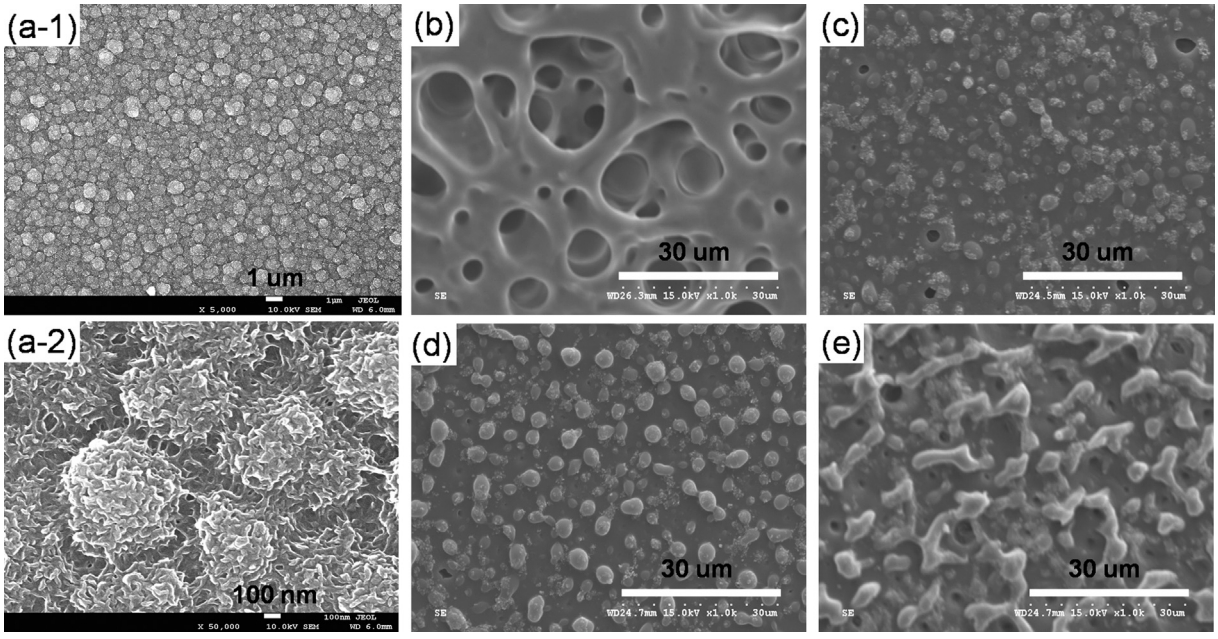

Fig. 2. SEM images of the PEDOT (a-1 and a-2), P-0 (b), P-500 (c), P-1000 (d), and P-1500 (e) CEs, respectively.

H out-of-plane deformation vibration, respectively. The characteristic peaks at 1685 cm^{-1} is responsible for the C=O bending in the COOH and the peak at 1160 cm^{-1} is due to the C–O–C stretching vibration [26,29,34]. The bands at 1585 and 1370 cm^{-1} are due to bending vibration of the thiophene ring, and 1140 and 1040 cm^{-1} are assigned to SO_3 of the PSS [35]. The peak at 990 cm^{-1} is attributed to a bending mode of the C–H on aromatic rings of the PSS [35].

In the P-1000 curve, the above characteristic peaks of PEDOT and PAA–PSS are all reflected in the spectrum of the P-1000. However, they have some shift or disappearance, indicating that the backbone structure of PEDOT and PAA–PSS were not damaged by the electrochemical polymerization. The FTIR spectra therefore indicate that the P-1000 thin films were successfully formed onto the FTO glass substrates.

3.2. Absorbency and ionic conductivity analysis

The absorbency of CEs and ionic conductivity (σ) of quasi-solid-state electrolytes were measured and listed in Table 1. From the table, the absorbency decreased with increasing the duration time of PEDOT electropolymerization, this is owing to the columnar PEDOT was gradually filling into the microporous 3D PAA–PSS network, which would cut down the inner space for the liquid electrolyte absorption [36]. The σ increased firstly and then decreased with the increase of duration time, this depends primarily on two factors: on the one hand, the introduction of proper-size columnar PEDOT could add many electron transport channels in the microporous 3D PAA–PSS network [24], which enhanced the σ; on the other hand, too much duration time brought about the columnar PEDOT overgrowth, and then cut down the absorbency of the 3D PAA–PSS network, which reduced the σ. As a result, the P-1000 achieved an absorbency of 12.65 g g^{-1} and σ of 10.59 mS cm^{-1}, respectively.

3.3. Electrocatalytic activity analysis

The CV measurements (Fig. 4) display that all the CEs have a pair of oxidation and reduction peaks, this redox pair is attributed to the reaction $I_3^- + 2e^- \rightarrow 3I^-$, which directly affects the DSSC performance [37,38]. The PEDOT CE (Fig. 4a) shows the largest anodic and cathodic current densities among these five CEs, this is due to the highest electrocatalytic activity for I_3^- reduction from the highly specific surface of nano-PEDOT and the highest σ of the liquid electrolyte. However, Fig. 4b reveals a lowest redox current densities in the P-0 CE, this is because of the hindrance of polymeric thickener or polymeric networks for the σ. It can be seen that the redox current densities increased firstly and then decreased with increasing the duration time (from Fig. 4c–e), this is due to the proper-size columnar PEDOT enhanced the catalytic activity of the CE and improved the σ of the 3D PAA–PSS network. However, the oversize PEDOT obviously reduced the σ of the 3D PAA–PSS network. The CV experiments are consistent with the σ results. The redox current densities of the P-1000 CE were close to those of the PEDOT CE, indicating the former would obtain a high photocurrent as well as the latter.

Table 1
Absorbency and ionic conductivity (σ) of the dual function polymer hybrid materials.

Samples	σ (mS cm^{-1}) (20 °C)	Absorbency (g g^{-1})
P-0	7.56	14.34
P-500	8.62	13.47
P-1000	10.59	12.65
P-1500	9.87	10.92

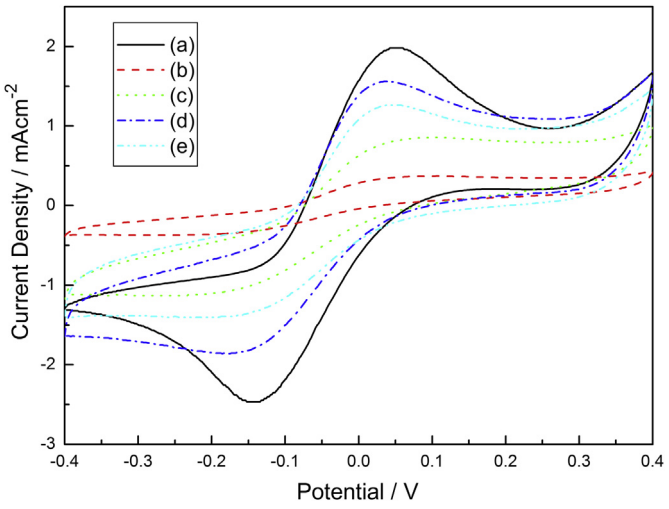

Fig. 4. CVs of the PEDOT (a), P-0 (b), P-500 (c), P-1000 (d), and P-1500 (e) CEs, respectively.

The EIS measurements were further carried out to evaluate the electrocatalytic activity of CEs and the σ of the electrolyte by measuring the charge-transfer resistance (R_{CT}). Fig. 5 represents the Nyquist plots of the PEDOT and dual function polymer hybrid CEs. Table 2 shows the impedance parameters obtained from the EIS data by using the Z-view software. The PEDOT CE demonstrates the best impedance properties among these five CEs, this is mainly attributed the highest σ of the liquid electrolyte. Compared to the dual function CEs, the P-1000 CE demonstrated impressive electrocatalytic activities. From Fig. 5b–e, the R_{CT} increases in the order of P-1000 (3.46 Ω cm^2) < P-1500 (4.37 Ω cm^2) < P-500 (5.11 Ω cm^2) < P-0 (5.29 Ω cm^2), indicating an inverse order of electrocatalytic activity of CEs [41,42] and the σ of quasi-solid-state electrolytes. Additionally, the constant phase element (CPE) is frequently used as a substitute for the capacitor in an equivalent circuit when the double layer does not behave as an ideal capacitor [39]. The CPE magnitude (Y_{CPE}) increases in the order of P-0 (4.87 mF cm^{-2}) < P-1500 (5.11 mF cm^{-2}) < P-500 (5.14 mF cm^{-2}) < P-1000 (5.94 mF cm^{-2}), demonstrating a same order of the active surface area of CEs, which is an important

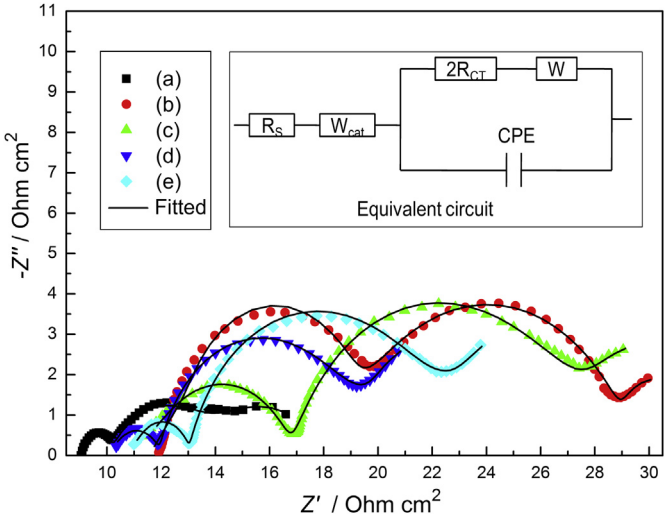

Fig. 5. Nyquist plots of the symmetrical PEDOT (a), P-0 (b), P-500 (c), P-1000 (d), and P-1500 (e) CEs, respectively.

Table 2
Best-fit values for R_S, W_{cat}, R_{CT}, W, and Y_{CPE} of the equivalent circuits to the impedance spectra in Fig. 5, and the photovoltaic performance of QS-DSSCs with different CEs.

CE	R_S (Ω cm^2)	W_{cat} (Ω cm^2)	R_{CT} (Ω cm^2)	W (Ω cm^2)	Y_{CPE} (mF cm^{-2})	J_{sc} (mA cm^{-2})	V_{oc} (mV)	FF	η (%)
(a)	9.04	1.44	1.52	3.98	2.42	13.67	741	0.65	6.58
(b)	11.55	7.33	5.29	8.53	4.87	12.87	753	0.52	5.04
(c)	10.64	6.17	5.11	6.10	5.14	13.17	755	0.56	5.57
(d)	9.91	2.03	3.46	5.85	5.94	13.52	758	0.62	6.35
(e)	10.26	2.36	4.37	7.70	5.11	13.39	756	0.59	5.97

contribution to the electrocatalytic activity. These are in consistence with the SEM, σ, and CV tests. The intercept of the real axis at high frequency is the ohmic series resistance (R_S) including the sheet resistance of two identical CEs and the electrolytic resistance, while the semicircle at low frequency represents the Warburg impedance (W) corresponding to the diffusion resistance of the I^-/I_3^- redox species. It should be noted that the Warburg impedance of the polymer-based CE originating from the charge transport in the catalyst cannot be ignored, due to its low electrical conductivity. Therefore, an element (W_{cat}) representing the Warburg impedance from the charge transport resistance in the polymer film should be introduced to the equivalent circuit [40]. The equivalent circuit model (inset in Fig. 5) was employed to simulate the resultant from the EIS measurements. As a result, the P-1000 CE had relatively low W (5.85 Ω cm^2) and W_{cat} (2.03 Ω cm^2).

Furthermore, Tafel polarization curves (Fig. 6) were measured to confirm the catalytic activities of various CEs and σ of quasi-solid-state electrolytes. The slopes for the anodic or cathodic branches are in the order of PEDOT > P-1000 > P-1500 > P-500 > P-0. A larger slope indicates a higher exchange current density (J_0) on the CE, the higher the J_0 and the more catalytically active the material [43]. J_0 can be also calculated by Eq. (2), where R_{CT} is the charge-transfer resistance obtained from EIS spectra, R is the gas constant, T is the temperature, n is the number of electrons involved in the reaction at the electrode, and F is Faraday's constant.

$$R_{CT} = \frac{RT}{nFJ_0} \tag{2}$$

In addition, at a low sweep rate, the limiting diffusion current density (J_{lim}) depends on the diffusion coefficient of the redox couple in the electrolyte, which can be expressed by Eq. (3) [43], where C is the concentration of I_3^-, D is the diffusion coefficient of the I_3^-, l is the space thickness, n and F have been defined previously.

$$J_{lim} = \frac{2nFC}{l}D \tag{3}$$

As the value of J_{lim} decreases in the order of PEDOT > P-1000 > P-1500 > P-500 > P-0 and is directly proportional to the D, explaining the P-1000 CE exhibited a lower electrocatalytic activity and σ than those of the PEDOT CE but higher than those of others dual function CEs. These Tafel polarization experiments are consistent with the EIS results.

3.4. Photovoltaic performance of DSSCs

Fig. 7 compares the photovoltaic characteristics of DSSCs based on various CEs under full sunlight illumination (100 mW cm^{-2}, AM1.5 G), and the resultant photovoltaic parameters were summarized in Table 2. The QS-DSSCs based on the dual function CEs showed little lower short-current density (J_{sc}) and higher open circuit voltage (V_{oc}) than those of the DSSC based on the PEDOT CE, this is due to the very thin quasi-solid-state electrolyte layer is good for obtaining perfect interface contact between dye-sensitized TiO_2 film and counter electrode [13]. By comparing the photovoltaic performances of various dual function CEs, the P-1000 CE demonstrated an enhancement of J_{sc} and V_{oc}, this possibly results from its high cathodic current density and enhanced diffusivity of I^-/I_3^- redox couple, as indicated in the aforementioned CV and σ tests [44,45]. The improvement on FF can be attributed to the slightly lower R_{CT} at electrolyte/CE interface and the much lower W of I_3^- in the electrolyte [42,44,46], these results are consistent with the EIS and Tafel polarization experiments. Therefore, the QS-DSSC assembled with the P-1000 CE exhibited a J_{sc} of 13.52 mA cm^{-2},

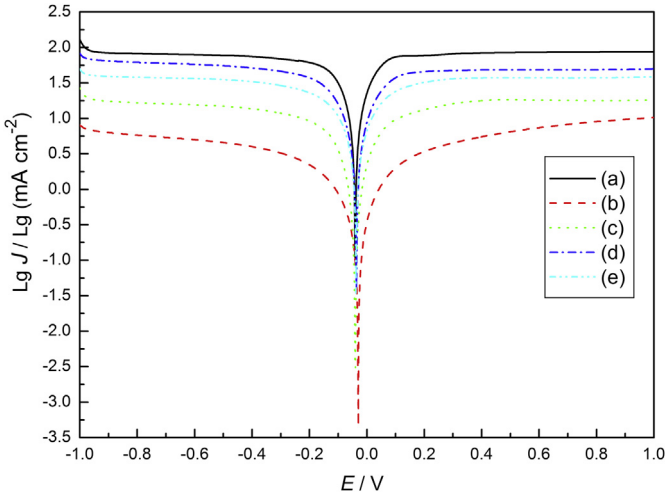

Fig. 6. Tafel curves of the symmetrical PEDOT (a), P-0 (b), P-500 (c), P-1000 (d), and P-1500 (e) CEs, respectively.

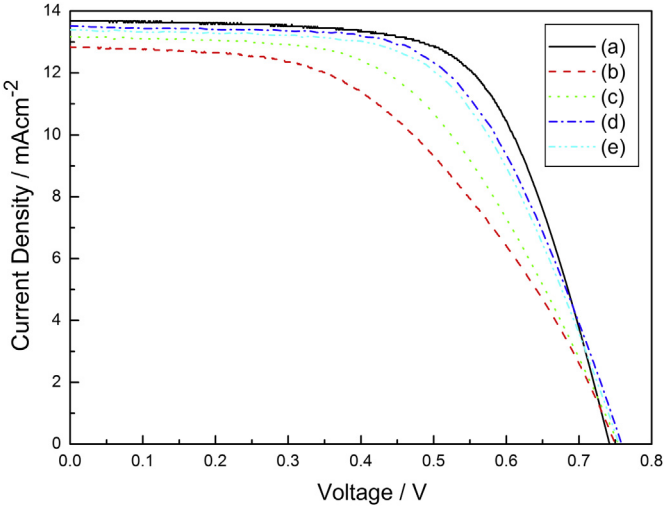

Fig. 7. Photocurrent density–voltage characteristics of the PEDOT (a), P-0 (b), P-500 (c), P-1000 (d), and P-1500 (e) CEs, respectively.

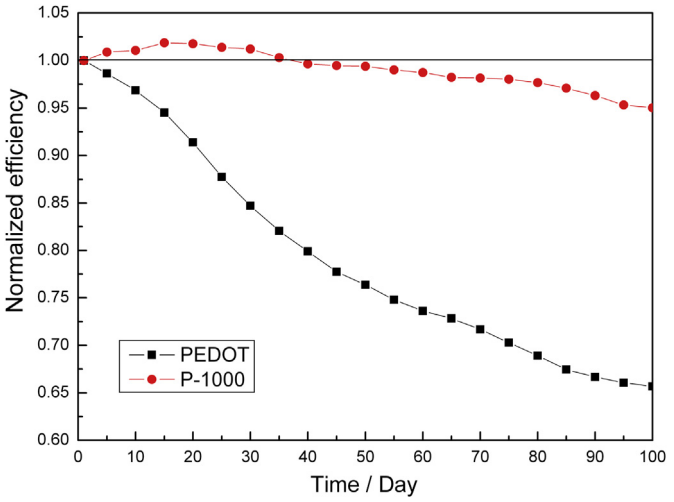

Fig. 8. Time-course changes of the normalized efficiency of the DSSC with PEDOT CE and QS-DSSC with P-1000 CE, respectively.

V_{oc} of 758 mV, FF of 0.62, and cell efficiency (η) of 6.35%, which were quite close to those of the PEDOT CE.

Fig. 8 shows the QS-DSSC based on the P-1000 CE exhibited much better stability than that of the DSSC based on the PEDOT CE. The η values were normalized to those of fresh ones. During the first twenty days, the η of the QS-DSSC increased slightly, this is due to the penetration of quasi-solid-state electrolyte through the nanoporous dye-sensitized TiO_2 photoanode [13]. The interfacial contact was enhanced by storing cells for some days, thus the performance of cells became better. The η of the QS-DSSC reduced to 6.03% after 100 days, while the DSSC fell to 4.34%, indicating the QS-DSSC had a better long-term stability, this is owing to the high absorbent ability of PAA–PSS hybrid for liquid electrolytes and the absorbed liquid electrolytes were hard to be leaked and volatilized for a long time.

4. Conclusion

In summary, a dual function polymer hybrid material was successfully fabricated both as a CE for I_3^- reduction and for storage of the liquid electrolyte in the QS-DSSC, which showed an excellent electrocatalytic activity and low R_{CT} of 3.46 Ω cm^2. The conversion efficiency of this QS-DSSC reached 6.35% under full sunlight illumination (100 mW cm^{-2}, AM1.5 G), which was quite close to that of the DSSC with the PEDOT CE (6.58%). The efficiency reduced to 6.03% after 100 days, indicating this QS-DSSC had a good long-term stability. Meanwhile, the liquid electrolyte could transform into the quasi-solid-state electrolyte after it was injected into the assembled DSSC, which would make the assembly process simply to achieve well-sealing and good long-term stable QS-DSSCs. As a result, this new kind of polymer hybrid material for stable QS-DSSCs should accelerate the practical application of DSSCs.

Acknowledgments

The authors are very grateful to the National High Technology Research and Development Program of China (No. 2009AA03Z217) and the National Natural Science Foundation of China (No. 90922028, 51002053). We also thank the joint support of the National Science Council in Taiwan for their financial supports under contract no. NSC-100-2221-E-036-022.

References

[1] B. O'Regan, M. Grätzel, Nature 353 (1991) 737.
[2] M. Grätzel, Inorg. Chem. 44 (2005) 6841.
[3] M. Grätzel, Acc. Chem. Res. 42 (2009) 1788.
[4] A. Hagfeldt, G. Boschloo, L. Sun, L. Kloo, H. Pettersson, Chem. Rev. 110 (2010) 6595.
[5] R. Trevisan, M. Döbbelin, P.P. Boix, E.M. Barea, R. Tena-Zaera, I. Mora-Seró, J. Bisquert, Adv. Energy Mater. 1 (2011) 781.
[6] N. Balis, T. Makrisa, V. Dracopoulosb, T. Stergiopoulosc, P. Lianos, J. Power Sources 203 (2012) 302.
[7] Y. Xiao, J. Lin, J. Wu, S. Tai, G. Yue, Electrochim. Acta 83 (2012) 221.
[8] Y. Xiao, J. Lin, S. Tai, S. Chou, G. Yue, J. Wu, J. Mater. Chem. 22 (2012) 19919.
[9] G. Smestad, C. Bignozzi, R. Argazzi, Sol. Energy Mater. Sol. Cells 32 (1994) 259.
[10] T. Yohannes, O. Inganäs, Sol. Energy Mater. Sol. Cells 51 (1998) 193.
[11] Q. Wang, J. Moser, M. Grätzel, J. Phys. Chem. B 109 (2005) 14945.
[12] J. Wu, S. Hao, Z. Lan, J. Lin, M. Huang, Y. Huang, L. Fang, S. Yin, T. Sato, Adv. Funct. Mater. 17 (2007) 2645.
[13] J. Wu, Z. Lan, J. Lin, M. Huang, S. Hao, T. Sato, S. Yin, Adv. Mater. 19 (2007) 4006.
[14] H. Lu, Y. Lee, S. Huang, C. Su, T. Yang, Sol. Energy Mater. Sol. Cells 95 (2011) 158.
[15] B. O'Regan, F. Lenzmann, R. Muis, J. Wienke, Chem. Mater. 14 (2002) 5023.
[16] P. Prene, E. Lancelle-Beltran, C. Boscher, P. Belleville, P. Buvat, C. Sanchez, Adv. Mater. 18 (2006) 2579.
[17] J. Wu, S. Hao, Z. Lan, J. Lin, M. Huang, Y. Huang, P. Li, S. Yin, T. Satot, J. Am. Chem. Soc. 130 (2008) 11568.
[18] I. Chung, B. Lee, J. He, R. Chang, M. Kanatzidis, Nature 485 (2012) 486.
[19] P. Wang, S. Zakeeruddin, J. Moser, M. Grätzel, J. Phys. Chem. B 107 (2003) 13280.
[20] P. Wang, S. Zakeeruddin, R. Humphry-Baker, M. Grätzel, Chem. Mater. 16 (2004) 2694.
[21] L. Stathatos, E. Zakeeruddin, S. Liska, P. Grätzel, Chem. Mater. 15 (2003) 1825.
[22] Z. Lan, J. Wu, S. Hao, J. Lin, M. Huang, Y. Huang, Energy Environ. Sci. 2 (2009) 524.
[23] S. Agarwala, C. Peh, G. Ho, ACS Appl. Mater. Interfaces 3 (2011) 2383.
[24] Z. Tang, J. Wu, Q. Liu, M. Zheng, Q. Tang, Z. Lan, J. Lin, J. Power Sources 203 (2012) 282.
[25] M. Biancardo, K. West, F.C. Krebs, Sol. Energy Mater. Sol. Cells 90 (2006) 2575.
[26] Z. Tang, J. Wu, Q. Li, Z. Lan, L. Fan, J. Lin, M. Huang, Electrochim. Acta 55 (2010) 4883.
[27] Z. Tang, Q. Liu, Q. Tang, J. Wu, J. Wang, S. Chen, C. Cheng, Electrochim. Acta 58 (2011) 52.
[28] Q. Li, J. Wu, Z. Tang, Y. Xiao, M. Huang, J. Lin, Electrochim. Acta 55 (2010) 2777.
[29] T. Mudiyanselage, D. Neckers, Soft Matter 4 (2008) 768.
[30] J. Wu, Y. Xiao, G. Yue, Q. Tang, J. Lin, M. Huang, Y. Huang, L. Fan, Z. Lan, S. Yin, T. Sato, Adv. Mater. 24 (2012) 1884.
[31] C. Kvarnstrom, H. Neugebauer, S. Blomquist, H. Ahonen, J. Kankare, A. Ivaska, N. Sariciftci, Synth. Met. 101 (1999) 66.
[32] C. Kvarnstrom, H. Neugebauer, A. Ivaska, N.S. Sariciftci, J. Mol. Struct. 521 (2000) 271.
[33] M. O'Connell, P. Boul, L. Ericson, C. Huffman, Y. Wang, E. Haroz, C. Kuper, J. Tour, K. Ausman, R. Smalley, Chem. Phys. Lett. 342 (2001) 265.
[34] Q. Tang, J. Wu, Q. Li, J. Lin, Polymer 49 (2008) 5329.
[35] Z. Wang, T. Sasaki, M. Muramatsu, Y. Ebina, T. Tanaka, L. Wang, M. Watanabe, Chem. Mater. 15 (2003) 807.
[36] S. Wang, M. Yaszemski, J. Gruetzmacher, L. Lu, Polymer 49 (2008) 5692.
[37] X. Mei, S. Cho, B. Fan, J. Ouyang, Nanotechnology 21 (2010) 395202.
[38] Z. Huang, X. Liu, K. Li, D. Li, Y. Luo, H. Li, W. Song, L. Chen, Q. Meng, Electrochem. Commun. 9 (2007) 596.
[39] X. Wu, H. Ma, S. Chen, Z. Xu, A. Sui, J. Electrochem. Soc. 146 (1999) 1847.
[40] J. Chen, B. Li, J. Zheng, J. Zhao, H. Jing, Z. Zhu, Electrochim. Acta 56 (2011) 4624.
[41] A. Fujiwara, Y. Matsuoka, Y. Matsuoka, H. Suematsu, N. Ogawa, K. Miyano, H. Kataura, Y. Maniwa, S. Suzuki, Y. Achiba, Carbon 42 (2004) 919.
[42] G. Mor, K. Shankar, M. Paulose, O. Varghese, C. Grimes, Nano Lett. 6 (2006) 215.
[43] M. Wang, A. Anghel, B. Marsan, N.-L. Cever Ha, N. Pootrakulchote, S. Zakeeruddin, M. Grätzel, J. Am. Chem. Soc. 131 (2009) 15976.
[44] Y. Saito, W. Kubo, T. Kitamura, Y. Wada, S. Yanagida, J. Photochem. Photobiol. A 164 (2004) 153.
[45] J. Lin, J. Liao, J. Electrochem. Soc. 159 (2012) D65.
[46] E. Ramasamy, W. Lee, D. Lee, J. Song, J. Power Sources 165 (2007) 446.